EUROPEAN ORGANIZATION FOR NUCLEAR RESEARCH

CERN-EP/85-170
22 October 1985

INCLUSIVE PHOTOPRODUCTION OF ϕ, $K^*(890)$ AND $K^*(1420)$ IN THE PHOTON ENERGY RANGE 20 TO 70 GeV

Omega Photon Collaboration

M. Atkinson[7], T.J. Axon[5], D. Barberis[5], T.J. Brodbeck[4], G.R. Brookes[8], J.J. Bunn[8], P.J. Bussey[3], A.B. Clegg[4], J.B. Dainton[3], M. Davenport[7], B. Dickinson[5], B. Diekmann[1], A. Donnachie[5], R.J. Ellison[5], P. Flower[7], P.J. Flynn[4], W. Galbraith[8], K. Heinloth[1], R.C.W. Henderson[4], R.E. Hughes-Jones[5], J.S. Hutton[7], M. Ibbotson[5], H.-P. Jakob[1], M. Jung[1], B.R. Kumar[7], J. Laberrigue[6], G.D. Lafferty[5], J.B. Lane[5], J.-C. Lassalle[2], J.M. Lévy[6], V. Liebenau[1], R.H. McClatchey[8], D. Mercer[5], J.A.G. Morris[7], J.V. Morris[7], D. Newton[4], C. Paterson[3], G.N. Patrick[2], E. Paul[1], C. Raine[3], M. Reidenbach[1], H. Rotscheidt[1], A. Schlösser[1], P.H. Sharp[7], I.O. Skillicorn[3], K.M. Smith[3], K.M. Storr[2], R.J. Thompson[5], Ch. de la Vaissière[6], A.P. Waite[5], M.F. Worsell[5] and T.P. Yiou[6]

Bonn[1]-CERN[2]-Glasgow[3]-Lancaster[4]-Manchester[5]-Paris VI[6]-Rutherford[7]-Sheffield[8]

ABSTRACT

Inclusive photoproduction of ϕ, $K^{*o}(890)$, $\bar{K}^{*o}(890)$ and $K^{*o}(1420)$, $\bar{K}^{*o}(1420)$ has been studied in γp collisions with photons of energy 20 to 70 GeV and in the range $0.1 \leq x_F \leq 0.95$ [$0.4 \leq x_F \leq 0.8$ for the $\overset{(-)}{K}{}^*(1420)$], x_F being the Feynman variable of the vector/tensor meson. The cross-sections for these processes, averaged over the photon energy range and integrated over x_F are given. The inclusive ϕ production in the forward direction can be described quantitatively by a triple-Regge model calculation. The remaining ϕ production and the total $K^{*o}(890)$ and $\bar{K}^{*o}(890)$ production are consistent with a quark fusion picture.

(To be submitted to Zeitschrift für Physik C)

0025P/EP/sm

1. INTRODUCTION

In this paper we report on the measurement of the inclusive processes

$$\gamma p \to \phi X \quad , \quad \phi \to K^+K^- \tag{1}$$

and

$$\gamma p \to K^{*o}(890)X \quad , \quad K^{*o}(890) \to K^+\pi^- \tag{2a}$$

$$\to \bar{K}^{*o}(890)X \quad , \quad \bar{K}^{*o}(890) \to K^-\pi^+ \tag{2b}$$

$$\gamma p \to K^{*o}(1420)X \quad , \quad K^{*o}(1420) \to K^+\pi^- \tag{3a}$$

$$\to \bar{K}^{*o}(1420)X \quad , \quad \bar{K}^{*o}(1420) \to K^-\pi^+ \tag{3b}$$

where X is a system of at least two particles with a mass greater than the sum of the proton and the pion mass.

The data originate from a general study of photoproduction of multiparticle final states carried out at the CERN SPS using the Omega Prime Spectrometer with a tagged photon beam in the energy range E_γ = 20–70 GeV (experiment WA57). The vector meson production was studied over the forward hemisphere in the overall centre-of-mass system in terms of the kinematical variables $x_F = p_L^*/p_{max}^*$ (where p_L^* is the momentum of the vector meson parallel to the photon beam direction in the c.m.s.) in the range from 0.1 to 0.95 and p_T^2, the square of the momentum of the vector meson perpendicular to the photon beam direction.

With the study of inclusive ϕ and K^* photoproduction we extend our previous study on inclusive ρ and ω photoproduction[1] to vector mesons containing strange quarks. While inclusive production of ϕ and K^* has been studied over a wide kinematical range with hadron[2] and lepton[3] beams, photoproduction data are rare. Two experiments have reported on inclusive photoproduction of ϕ, between 25 and 70 GeV [4] and 4.6–6.7 GeV [5], and one experiment on inclusive photoproduction of $K^{*o}(890)$, $\bar{K}^{*o}(890)$ at 20 GeV [6].

The study presented here overlaps with and extends the previous study of Ref. 4. The study of $K^*(890)$ vector meson production is completely new. The present results together with those of Ref. 1 provide a comparison of inclusive photoproduction between particles containing only u and d quarks on the one hand (ρ and ω) [1] and the ϕ with $s\bar{s}$ content on the other.

Integrated cross-sections of $K^{*o}(1420)$ and $\bar{K}^{*o}(1420)$ tensor meson production in a restricted x_F range are reported for the first time in photoproduction.

2. EXPERIMENT AND DATA SELECTION

The data were obtained at the CERN SPS as part of a photoproduction experiment using a tagged photon beam and the Omega Prime Spectrometer. The experimental details can be found elsewhere[7]. The primary photons were tagged in the momentum range 20 to 70 GeV and hit a 600 mm liquid hydrogen target. Charged particles were measured by MWPCs in the spectrometer and π^os were measured via their decay into two photons by a lead glass wall. Charged kaons and protons/antiprotons were identified within the momentum range $5 \leq p_K \leq 18$ GeV/c and $19 \leq p_p \leq 35$ GeV/c, respectively, by means of a threshold gas Cerenkov counter. Recoil protons were identified in the range $0.2 \leq p_p \leq 1$ GeV/c by measuring their energy loss dE/dx in a scintillation counter[8]. All particles not positively identified as kaons or protons were considered to be pions. The data sets for this analysis came from two different triggers in the experiment:

i) A trigger (T1) which required a charged multiplicity between three and eight in the detector downstream of the target and at least one particle with no light in the Cerenkov counter, indicating consistency with a charged kaon/nucleon track. This trigger yielded the event sample with a $K^{\pm}$ in the final state and also, as a subsample, that with an identified K^+K^- pair.

ii) A trigger (T2) which required a charged forward multiplicity of two and no signal from a device sensitive to e^+e^- pairs. This low

multiplicity trigger provided, besides pionic final states (not considered here), the elastic ϕ production reaction

$$\gamma p \to \phi p \quad , \quad \phi \to K^+K^-$$

and inelastic reactions containing charged kaons, essentially

$$\gamma p \to K^+K^- (m\pi^o)p \quad , \quad m \geq 1 \ .$$

From the interaction of 5.63×10^{10} photons within the tagging range, incident on 2.54×10^{24} protons/cm^2 of hydrogen, corresponding to a luminosity of 143 nb^{-1}, totals of $\sim 3 \times 10^6$ events (T1) and $\sim 1 \times 10^6$ events (T2) were recorded.

In the data reduction we required for both triggers a well measured primary photon in the designed energy range ($20 \leq E_\gamma \leq 70$ GeV), the event vertex to be inside the hydrogen target, an event multiplicity consistent with the trigger conditions and a well classified charged kaon track ($5 \leq p_K \leq 18$ GeV/c). The background of protons and antiprotons taken as $K^\pm$ was less than 10%. Elastic production, which contributes to T2 events, was excluded by requiring $m_X^2(K^+K^-) \geq 2$ GeV/c^2, $m_X^2(K^+K^-)$ being the mass squared recoiling against the K^+K^- system in an event. This cut removes essentially K^+K^- events with $x_F(K^+K^-) \geq 0.95$, covering the elastic ϕ production.

The selected event samples contained finally $\sim 1.7 \times 10^6$ events with a well identified K^+ or K^- (data set 1) and, as a subsample, $\sim 7.1 \times 10^4$ events with an identified K^+K^- pair (data set 2).

Invariant mass spectra of K^+K^- and $K^\pm\pi^\mp$ combinations for the various data sets are shown in Figs. 1, 2a,b. To determine the number of events for total and differential cross-sections of ϕ, $K^*(890)$ and $K^*(1420)$, appropriate fits to the relevant mass spectra were carried out in each case (see Section 4).

3. ACCEPTANCE

Three major effects had to be taken into account in determining the acceptance:

i) the effects of the trigger requirements;

ii) the efficiency of charged kaon identification due to the performance of the Cerenkov counter;

iii) the precision of measurement of single tracks which have to be reconstructed in order to form the KK and Kπ mass combinations, respectively.

The acceptance was determined on a 5 × 10 grid in E_γ and x_F of the vector meson (ΔE_γ = 10 GeV, Δx_F = 0.1) by applying a nearly model-independent method. Real events were rotated in 12 equidistant steps around the photon beam axis. At each step the resonance decay particles were additionally rotated in the φ and K^* rest system, respectively, computing the kaon (pion) momentum for 32 fixed equidistant combinations of helicity angles ($\cos\theta_H, \phi_H$).

It was assumed that the decay angular distributions are flat in the s-channel helicity system, an assumption which is justified experimentally (see below). This double rotation method generated, from one real event, 384 artificial events which were then processed through the program MAP [9]. This program simulates the experimental set-up in all essential details including the trigger requirements and the performance of the Cerenkov counter for the charged kaon identification.

The fraction of these events fulfilling all acceptance criteria provided a probability estimate for the single event being accepted. The resulting mean acceptance values averaged over the E_γ range 20–70 GeV and the x_F range $0.1 \leq x_F \leq 0.95$ [$0.4 \leq x_F \leq 0.8$ only in the $(\bar{K})^*(1420)$ case] were found to be

$$A(\phi \to K^+K^-) = (21.5 \pm 1.4)\%$$

$$A[\overset{(-)}{K}{}^{*o}(890) \to \pi^{\pm}K^{\mp}] = (28.7 \pm 1.5)\%$$

$$A[\overset{(-)}{K}{}^{*o}(1420) \to \pi^{\pm}K^{\mp}] = (26.0 \pm 2.0)\% \ .$$

The errors include our estimates of systematic uncertainties. In particular it was checked that the acceptance values are not sensitive to the assumption of a flat decay angular distribution. Experimentally the K^* decay angular distributions are found to be flat and the ϕ decay angular distributions deviate significantly from isotropy only at high x_F.

4. EXPERIMENTAL RESULTS

4.1 Integrated cross-sections

In order to measure the inelastic resonance signals the mass distributions in Figs. 1 and 2 were fitted to

$$\frac{d\sigma}{dM} = a \cdot BW(M) + b \cdot BG(M)$$

where the resonance shape was taken as a Breit-Wigner function of the form

$$BW(M) = \frac{M \cdot M_R \cdot \Gamma(M)}{(M^2 - M_R^2)^2 + M_R^2 \cdot \Gamma^2(M)}$$

with resonance mass M_R and a mass-dependent width of the form

$$\Gamma(M) = \Gamma_R \cdot \left(\frac{q}{q_R}\right)^{2\ell+1} \cdot \frac{\rho(M)}{\rho(M_R)}$$

where

$$\rho(M) = \frac{1}{q_R^2 + q^2} \ .$$

Γ_R is the resonance width, q the three momentum of the decay products in the resonance rest frame, q_R the value of q at the resonance mass and

ℓ the relative angular momentum of the decay particles. For the background distribution BG(M) we have chosen a 3rd order polynomial in the case of the ϕ and for the K^*'s we used an exponential with a threshold factor

$$BG(M) = (M-M_{THR})^{\alpha} \cdot \exp(-\beta M^2 - \gamma M) ,$$

M_{THR} being the threshold mass and α, β, γ being determined by the fit. Because of the positive kaon identification, the ρ reflection under the K^* is less than 5% of the K^* signal. There is in principle a reflection from highly asymmetric decays of the ϕ, but this is negligible.

The fit for the ϕ signal in the full data [$20 \leq E_\gamma \leq 70$ GeV, $0.1 \leq x_F(\phi) \leq 0.95$, all $p_T^2(\phi)$] is shown in Fig. 1 and the resulting mass, width and number of ϕ's are given in Table 1. The width is consistent with our experimental resolution. The inclusive ϕ photoproduction cross-section was calculated taking into account the total luminosity of 143 nb^{-1} (see Section 2), the acceptance factor of Section 3 and another acceptance factor accounting for various further (overall) inefficiencies in the beam line, the tagging system and the event reconstruction software. After correcting for the branching ratio $BR(\phi \rightarrow K^+K^-) = (0.493 \pm 0.01)$ [10], the cross-section averaged over the whole photon energy range and integrated over $0.1 \leq x_F \leq 0.95$ and all p_T^2 was found to be

$$\sigma(\gamma p \rightarrow \phi + X) = (1.499 \pm 0.074 \pm 0.150)\ \mu b$$

where the errors correspond to statistical and systematic uncertainties, respectively. In the more restricted x_F range $0.2 \leq x_F \leq 0.8$ the integrated cross-section is

$$\sigma(\gamma p \rightarrow \phi + X) = (0.907 \pm 0.037 \pm 0.09)\ \mu b .$$

The previous experiment[4] with a slightly different energy range ($25 \leq E_\gamma \leq 70$ GeV) found for this x_F range a value of

$$\sigma(\gamma p \rightarrow \phi + X) = (0.621 \pm 0.033 \pm 0.19)\ \mu b .$$

Fits to the K^* mass spectra of Figs. 2a and b were carried out as described above, using a second Breit-Wigner formula for the $\overset{(-)}{K}{}^{*o}(1420)$ in the $\pi^{\pm}K^{\mp}$ distributions. The resulting masses and widths are given in Table 1. The cross-sections for K^* photoproduction were determined as described for the ϕ. For the $\overset{(-)}{K}{}^{*o}(890)$ in the x_F range $0.1 \leq x_F \leq 0.9$ integrated over p_T^2 and corrected for the branching ratio they are

$$\sigma(\gamma p \to K^{*o}(890) + X) = (3.33 \pm 0.19 \pm 0.40)\ \mu b$$

$$\sigma(\gamma p \to \bar{K}^{*o}(890) + X) = (3.29 \pm 0.20 \pm 0.39)\ \mu b\ .$$

We note that the inelastic cross-section for ϕ production is about 1/10 of the inelastic cross-section for ρ and ω production[1] whereas the inelastic K^* cross-sections are in between (1/3 of ρ and ω).

The $\overset{(-)}{K}{}^{*o}(1420)$ cross-sections, corrected for the branching ratio $K^*(1420) \to K\pi$ of (0.45 ± 0.02) [10], in the x_F range $0.4 \leq x_F \leq 0.8$ and over the total photon energy range were found to be

$$\sigma(\gamma p \to K^{*o}(1420) + X) = (0.224 \pm 0.054 \pm 0.03)\ \mu b$$

$$\sigma(\gamma p \to \bar{K}^{*o}(1420) + X) = (0.217 \pm 0.046 \pm 0.03)\ \mu b\ .$$

For the common x_F ranges $0.4 \leq x_F \leq 0.8$ the cross-section ratios are

$$\frac{\sigma[K^{*o}(1420)]}{\sigma[K^{*o}(890)]} = 0.36 \pm 0.09$$

$$\frac{\sigma[\bar{K}^{*o}(1420)]}{\sigma[\bar{K}^{*o}(890)]} = 0.31 \pm 0.07\ .$$

These ratios of tensor to vector meson production are consistent with those found with kaon beams (Refs. 2b,c,d,e) and pion beams[11].

4.2 Charged hadronic multiplicity and mass recoiling against the vector mesons

The inelasticity of ϕ and $K^*(890)$ was studied in terms of the charged hadronic multiplicity and of m_X^2, the mass squared recoiling

against the vector meson. The rates were determined by fitting corresponding mass spectra for the multiplicities from 3 to 11 and slices of m_X^2 and are shown together with the acceptance curves in Figs. 3 and 4.

The multiplicity and m_X^2 distributions for ϕ and $K^*(890)$ production are similar to each other and to the corresponding ones for inclusive ρ and ω production[1]. One would expect such a similarity in any model in which the production of the particles accompanying the vector meson is independent of its dynamics, and in which the dynamical mechanisms for the production of the different vector mesons are the same.

4.3 x_F and p_T^2 distributions

In the range $0.1 \leq x_F \leq 0.95$ for ϕ, $K^{*o}(890)$ and $\bar{K}^{*o}(890)$ the distributions of $d\sigma/dx_F$ and $F(x_F)$ were determined, $F(x_F)$ being the Lorentz invariant cross-section

$$F(x_F) = \frac{1}{\pi} \frac{E^*}{p^*_{max}} \frac{d\sigma}{dx_F}$$

where E^* and p^*_{max} are the energy and maximum possible momentum of the vector meson in the overall c.m.s. computed event by event.

The results for these distributions were obtained by dividing the data into three ranges of E_γ: 20-35 GeV, 35-50 GeV, 50-70 GeV. The distributions for the different E_γ ranges agree well, indicating that there is no significant variation of the cross-section with E_γ.

We present the results averaged over the total E_γ range in Table 2. The non-invariant cross-sections are also shown in Figs. 5 and 6. The x_F dependence of the ϕ agrees with that from the previous experiment[4]. In particular, there is a rise for $x_F \geq 0.75$, which can be interpreted as a contribution from diffractive dissociation of the photon into a ϕ state (see Section 5.1).

The distributions for inclusive $K^{*o}(890)$ and $\bar{K}^{*o}(890)$ production decrease with increasing x_F. The $K^{*o}/\bar{K}^{*o}$ cross-section ratio is shown in Fig. 7. It is consistent with being 1 throughout the x_F range. The dependence on p_T^2 for ϕ production is shown in Fig. 8. The distribution is well described by $d\sigma/dp_T^2 \sim e^{bp_T^2}$. The value of b was found to be $b = (-2.62 \pm 0.16)$ $(GeV/c)^{-2}$ and does not show a significant variation as a function of E_γ. It is in good agreement with the result of Ref. 4.

4.4 Decay angular distributions of the ϕ

The decay angular distribution of inclusively produced ϕ's has been studied in the s-channel helicity system[12], over the whole photon energy range and excluding the elastic reaction $\gamma p \to \phi p$. Figure 9 shows the distributions of $\cos\theta_H$ for all inelastic ϕ's (a) and for subsamples corresponding to $x_F \geq 0.7$ (b) and $x_F < 0.7$ (c). The distributions of the azimuthal angle ϕ_H were consistent with being flat (not shown).

The $\cos\theta_H$ distributions have been fitted to the form $a\cdot(1 + b\cos^2\theta_H)$. The resulting values of b are given in Table 3 in comparison with the results of Ref. 4, which were based on a more restrictive selection of ϕ's, namely ϕ's with $17 \leq p_{lab}(\phi) \leq 26$ GeV/c. The data indicate a large $\sin^2\theta_H$ component for $x_F \geq 0.7$, similarly as observed in elastic production of vector mesons. For $x_F < 0.7$ the value of b is consistent with zero indicating that some other production mechanism is dominant.

4.5 Strange particles being associated with inclusive ϕ production

From the data set defined by requiring ≥ 1 K^+ and ≥ 1 K^- in the final state (data set 2) the subsamples with another K^+, K^-, K^o_S or Λ in the final state were selected, and the number of ϕ's was computed by a fit to the mass distributions of the K^+K^- combinations of these events. Table 4a shows for the x_F range of the associated kaons $0.1 \leq x_F(K) \leq 0.5$ the number of ϕ's found in this experiment.

The numbers are not corrected for acceptance losses (which cannot be calculated in a straightforward manner due to the lack of an adequate model for the production mechanism) so that they have to be understood as lower limits. However, the detection probabilities for the strange particles are the same for K^+ and K^- due to the symmetry of the apparatus. It was checked that the shape of the x_F distributions of the accompanying $K^\pm$ are similar.

The single rates of K^+ and K^- events show a pronounced asymmetry of

$$A = \frac{N(\phi K^+) - N(\phi K^-)}{N(\phi K^+) + N(\phi K^-)} = 0.27 \pm 0.06 \ .$$

This ratio is only slightly biased by acceptance effects.

The asymmetry indicates an excess of K^+ events which could originate from K^+ + hyperon production (where the hyperon is not seen). The data (Table 4b) appear to show some energy dependence of the asymmetry varying as $A \sim E_\gamma^{-n}$, n being 1.9 ± 0.2.

5. DISCUSSION

5.1 Diffractive production of the ϕ

Guided by the results from inclusive ρ/ω production[1], the cross-section of inclusive ϕ production in the forward direction was compared with an estimate of diffractive ϕ production which was obtained from a triple-Regge model.

Assuming Pomeron dominance and Pomeron factorization the cross-section for $\gamma p \to \phi X$ within this model is given by

$$\frac{d^2\sigma}{dt dx_F} = \beta_{ppP}(0) \cdot \beta^2_{\gamma\phi P}(t) \cdot G_{PPP} \cdot \frac{1}{16\pi(1-x_F)}$$

and the diffractive cross-section for $\gamma p \to \phi p$ is given by

$$\frac{d\sigma}{dt} = \frac{1}{16\pi} \cdot \beta^2_{\gamma\phi P}(t) \cdot \beta^2_{ppP}(t) \ .$$

With the triple-Pomeron coupling $G_{PPP} \sim 0.32$ (mb GeV^{-2})$^{1/4}$ (Ref. 13), the proton-proton-Pomeron vertex factor at 40 GeV (Refs. 1,14)

$$\beta^2_{ppP}(t) = 51.3 \exp(-5|t|) \text{ (mb GeV}^{-2})^{1/2} \ ,$$

a ϕ forward differential cross-section of

$$\left.\frac{d\sigma}{dt}\right|_{t=o} = (2.41 \pm 0.4) \ \mu b/GeV^2 \text{ (Ref. 15)}$$

and an exponential t-slope of (6 ± 0.3) GeV^{-2} [s)] (the latter two from elastic ϕ production) we find

$$\frac{d\sigma}{dx_F} = (107.67^{+71.85}_{-38.52}) \cdot \frac{1}{1-x_F} \text{ nb} \ .$$

Figure 5 compares the experimental distribution $d\sigma/dx_F$ (ϕ) with this prediction (drawn in as a band, corresponding to the errors). For $x_F \geq 0.8$ the quantitative agreement is satisfactory.

5.2 Non-diffractive production of ϕ and $K^*(890)$

Non-diffractive vector meson production is known to be reasonably well described by the quark fusion model for hadron experiments[16)]. In this model the general expression for the cross-section of the reaction A + B → C + X is given by

$$\frac{2E}{\sqrt{s}} \frac{d\sigma}{dx_F} = \frac{4\pi^2}{3M_C^2} \sum_{q_1\bar{q}_2} \frac{g^2_{q_1\bar{q}_2}}{4\pi} \{F^{q_1}_{A1}(x_1)F^{\bar{q}}_{B2}(x_2) + F^{\bar{q}}_{A2}(x_1)F^{q_1}_{B1}(x_2)\} \ .$$

Here $F^q_A(x)$ and $F^q_B(x)$ are the quark distributions in the beam and target particle, respectively, with the sum running over all possible types of quarks $q_1, \bar{q}_2$ which couple to the meson C with coupling strength $g_{q_1\bar{q}_2}$. The fractional momenta of beam and target (x_1 and x_2, respectively) carried by the quarks are defined as usual: $x_1 - x_2 = x_F$, $x_1 \times x_2 = M_C^2/s$.

To extend this model to photoproduction the incoming photon is coupled via VMD to ρ^o, ω, ϕ, thus acting as an incoming hadron. It has been shown that the valence quark distributions of the vector meson are consistent with being those of the pion, i.e $\sim x(1-x)$ [1,4].

In the previous study of ϕ photoproduction[4] it was argued that for kinematical reasons predominantly valence quarks of the photon and sea quarks of the proton should contribute to the process (recombination type model). This picture described the data in a satisfactory way.

In this analysis we retained also contributions from photon sea quarks and proton valence quarks. Allowing for different contributions from u and d quarks with OZI violating coupling $\tilde{g}$ and from s quarks with a normal hadronic coupling g the cross-section for ϕ photoproduction within the quark fusion model reads

$$\frac{2E}{\sqrt{s}}\frac{d\sigma}{dx_F} = \frac{4\pi^2\alpha}{3M_\phi^2} \cdot \Big\{ \frac{3}{2}\frac{\tilde{g}^2}{4\pi}\left(\frac{4\pi}{f_\rho^2}+\frac{4\pi}{f_\omega^2}\right) V_\gamma(x_1)\cdot V_p(x_2)$$

$$+ 3\,\frac{\tilde{g}^2}{4\pi}\left(\frac{4\pi}{f_\rho^2}+\frac{4\pi}{f_\omega^2}+\frac{4\pi}{f_\phi^2}\right) S_\gamma(x_1)\cdot V_p(x_2)$$

$$+ 2\,\frac{\tilde{g}^2}{4\pi}\left[\frac{4\pi}{f_\rho^2}+\frac{4\pi}{f_\omega^2}+\lambda\,\frac{4\pi}{f_\phi^2}\left(1+\frac{g^2}{\tilde{g}^2}\right)\right] V_\gamma(x_1)\cdot S_p(x_2)$$

$$+ 2\,\frac{\tilde{g}^2}{4\pi}\left[2+\lambda^2\left(1+\frac{g^2}{\tilde{g}^2}\right)\right]\left(\frac{4\pi}{f_\rho^2}+\frac{4\pi}{f_\omega^2}+\frac{4\pi}{f_\phi^2}\right) S_\gamma(x_1)\cdot S_p(x_2)\Big\}.$$

Here V and S are the valence and sea quark distributions, respectively, $4\pi/f_{VM}^2$ are the VMD couplings of the photon to the vector meson VM and λ is the suppression factor of s quarks relative to u and d quarks in the sea. This formula is illustrated in the diagrams of Fig. 10.

The structure functions were taken from Moore[17] assuming those of the pion for the (vector meson dominated) photon. $\tilde{g}^2/g^2$ and λ were kept as parameters in a fit to the data. These data were obtained from the cross-sections in Table 2 by subtracting the diffractive part as estimated via the triple-Regge model of Section 5.1. The resulting distribution is shown in Fig. 11 together with a fitted curve which has been normalized to these data. The different contributions to this curve from the VV, SV, VS, and SS term, respectively, are shown separately in Fig. 12. The fit describes the data equally well for combinations of the unknown parameters in the ranges $0.1 \leq \lambda \leq 0.4$ and $0.01 \leq \tilde{g}^2/g^2 \leq 0.03$.

The range of $\tilde{g}^2/g^2$ leads to the conclusion that the OZI violating processes of inclusive ϕ production contribute between 25% and 50% for $\lambda = 0.25$ [18]. This conclusion is consistent with an independent estimate which can be obtained in terms of the quark fusion model. With unpolarized quarks the angular distribution of the K^+ in the Gottfried-Jackson frame is given by $C\cdot(1 + \alpha \cos^2 \theta)$ with $\alpha = -(1-4\cdot m_q^2/M_\phi^2)$, where m_q is the mass of the quark involved. We estimate from our data $\alpha \geq -0.2$ at 90% confidence level which corresponds to $\leq$ 30% OZI violating contributions.

Applying the quark fusion model to the photoproduction of K^{*o} and $\bar{K}^{*o}$ no contributions from OZI violating processes are possible at the same level considered for the ϕ. The lines in Fig. 6 show the prediction of the model in comparison with our data (height adjusted). The agreement in shape is satisfactory. Again this shape is nearly insensitive to a variation of λ in the range $0.1 \leq \lambda \leq 0.4$. The result of the model calculations for the cross-section ratio $d\sigma/dx_F$ $(K^{*o})/d\sigma/dx_F$ $(\bar{K}^{*o})$ is shown as the line in Fig. 7.

The similarity of K^{*o} and $\bar{K}^{*o}$ data indicates that contributions of proton valence quarks, which are possible for K^{*o} production ($\bar{s}d$ system), but not for $\bar{K}^{*o}$ production ($s\bar{d}$ system), are small. Further the $S_\gamma(x_1)\cdot S_p(x_2)$ contribution, mainly for $x_F <$

0.3, is in total about 40% of that from $V_\gamma(x_1) \cdot S_p(x_2)$ since only the valence $d\bar{d}$ and $s\bar{s}$ quarks can contribute to $V_\gamma(x_1)$, which account for 1/3 of the photon's valence quark content.

Within the accuracy of our data, it might be that the effect of producing the K^{*o} with valence quarks from the proton is not as important as might be expected from the simple quark fusion model. However, this requires knowledge of the proton valence quark distribution at small x ($\lesssim$ 0.1), where it is not well established[19]. This is an interesting point, which can be investigated further by also studying the photoproduction of $K^{*\pm}$.

6. SUMMARY

This paper reports on the inclusive photoproduction of ϕ, $\overset{(-)}{K}{}^{*o}(890)$ and $\overset{(-)}{K}{}^{*o}(1420)$ with photons of energy 20–70 GeV in the kinematical range $0.1 \leq x_F \leq 0.95$. The cross-section for the ϕ meson is (1.499 ± 0.074 ± 0.150) μb; its production over the whole x_F range is consistently described by a quark fusion model with an additional diffractive contribution for high x_F quantified by a triple-Regge mechanism. Integrated cross-sections for $K^{*o}(890)$, $\bar{K}^{*o}(890)$ production are measured to be equal and to be about 2.2 times bigger than for the ϕ. Again the quark fusion picture provides a satisfactory description of the production mechanism.

The first observation of $K^{*o}(1420)$, $\bar{K}^{*o}(1420)$ in photoproduction is reported. Its integrated cross-section over a restricted x_F range ($0.4 \leq x_F$ 0.8) is found to be ~ 1/3 of that for the corresponding $K^*(890)$ in the same kinematical range.

Acknowledgements

We are grateful to the Omega Group at CERN for their help in running the spectrometer and providing on-line and off-line software. The work of the technical support staff in our home institutes, and the support at the computer centres at the Rutherford Appleton Laboratory, CERN, and the RHRZ at Bonn have been invaluable. We thank the SERC (UK), the BMFT (Fed. Rep. Germany), and the IN2P3 (France) for financial support.

REFERENCES

1) M. Atkinson et al., Nucl. Phys. B245 (1984) 189.

2) a) M. Barth et al., Phys. Lett. 117B (1982) 267.
b) M. Barth et al., Nucl. Phys. B223 (1983) 296.
c) P.V. Chliapnikov et al., Nucl. Phys. B176 (1980) 303.
d) I.V. Ajinenko et al., Z. Phys. C 5 (1980) 177.
e) P.V Chliapnikov et al., Z. Phys. C 12 (1982) 113.
f) R. Göttgens et al., Z. Phys. C 12 (1982) 323.
g) H.G. Kirk et al., Nucl. Phys. B116 (1976) 99.
h) V. di Gennaro et al., Nucl. Phys. B173 (1980) 107.
i) D.H. Brick et al., Phys. Rev. D25 (1982) 2248.
j) P. Sixel et al., Nucl. Phys. B199 (1982) 381.
k) T. Akesson et al., Nucl. Phys. B203 (1982) 27.

3) a) W. Shambroom et al., Phys. Rev. D26 (1982) 1.
b) H. Graessler et al., Nucl. Phys. B194 (1982) 1.
c) H. Aihara et al., Phys. Rev. Lett. 52 (1984) 2201.
d) A. Cordier et al., Phys. Lett. 110B (1982) 335.

4) D. Aston et al., Nucl. Phys. B179 (1981) 215.

5) H.J. Behrend et al., Nucl. Phys. B144 (1978) 22.

6) K. Abe et al., Phys. Rev. D29 (1984) 1877.

7) Experiments at CERN in 1980 (CERN, Geneva, 1980); experiment WA57.

8) A. Schlösser, Univ. Bonn report IR-80-11 (1980).

9) A.P. Waite, MAP Program Guide, University of Manchester, unpublished.

10) M. Aguilar-Benitez et al., Rev. Mod. Phys. 56, No. 2 (1984).

11) W. Kittel in Proc. of X Int. Symp. on Multiparticle Dynamics, Goa (1979).

12) T.H. Bauer et al., Rev. Mod. Phys. 50, No. 2 (1978).

13) A. Donnachie and P.V. Landshoff, private communication.
M.G. Albrow et al., Nucl. Phys. B108 (1976) 1.

14) A. Donnachie and P.V. Landshoff, Nucl. Phys. B231 (1984) 189.

15) D. Aston et al., Nucl. Phys. B172 (1980) 1.

16) Y. Arestov et al., Z. Phys. C 8 (1981) 283.
C. Daum et al., Nucl. Phys. B186 (1981) 205.

17) R. Moore, J. Phys. G5 (1979) 1509.

18) P.K. Malhotra and R. Orava, Z. Phys. C 17 (1983) 85.
G.T. Jones et al., Z. Phys. C 27 (1985) 43.

19) F. Dydak in Proc. of 1983 Int. Symp. on Lepton and Photon Interactions at High Energies, Cornell University (1983), p. 634.

Table 1

Results of the fits to the K^+K^-, π^-K^+ and π^+K^- mass spectra of Figs. 1 and 2

Channel	M_R (MeV)	Γ_R (MeV)	No. of resonances
$\phi \rightarrow K^+K^-$	1020.1 ± 0.11	10.13 ± 0.31	5526 ± 132
$K^{*o}(890) \rightarrow \pi^-K^+$	894.52 ± 0.63	59.81 ± 2.29	25182 ± 855
$\bar{K}^{*o}(890) \rightarrow \pi^+K^-$	894.63 ± 0.76	62.60 ± 2.81	19927 ± 795
$K^{*o}(1420) \rightarrow \pi^-K^+$	1408.45 ± 6.22	62.68 ± 20.88	1402 ± 375
$\bar{K}^{*o}(1420) \rightarrow \pi^+K^-$	1435.39 ± 6.49	81.44 ± 23.81	1582 ± 380

Table 2

Non-invariant $d\sigma/dx_F$ and invariant $F(x_F) = 1/\pi\ E^*/P^*_{max}\ d\sigma/dx_F$ distributions for reactions (1), (2a), and (2b)

	$\gamma p \to \phi + X$		$\gamma p \to K^{*o}(890) + X$		$\gamma p \to \bar{K}^{*o}(890) + X$	
x_F interval	$\frac{d\sigma}{dx_F}$ (μb/0.1)	$F(x_F)$(μb/0.1)	$\frac{d\sigma}{dx_F}$ (μb/0.1)	$F(x_F)$(μb/0.1)	$\frac{d\sigma}{dx_F}$ (μb/0.1)	$F(x_F)$(μb/0.1)
0.1-0.2	3.41 ± 0.59	0.29 ± 0.11	11.09 ± 1.26	0.92 ± 0.23	9.14 ± 1.22	0.76 ± 0.19
0.2-0.3	2.41 ± 0.25	0.28 ± 0.05	9.16 ± 1.00	0.99 ± 0.19	10.12 ± 1.13	1.09 ± 0.21
0.3-0.4	1.90 ± 0.17	0.26 ± 0.04	6.31 ± 0.72	0.86 ± 0.14	6.26 ± 0.78	0.86 ± 0.14
0.4-0.5	1.50 ± 0.12	0.26 ± 0.03	2.76 ± 0.37	0.46 ± 0.07	3.17 ± 0.51	0.53 ± 0.10
0.5-0.6	1.14 ± 0.10	0.24 ± 0.03	1.63 ± 0.27	0.32 ± 0.06	1.60 ± 0.33	0.32 ± 0.07
0.6-0.7	0.95 ± 0.09	0.23 ± 0.03	1.00 ± 0.22	0.23 ± 0.05	1.37 ± 0.38	0.31 ± 0.09
0.7-0.8	1.16 ± 0.11	0.31 ± 0.03	0.93 ± 0.30	0.24 ± 0.08	0.86 ± 0.33	0.22 ± 0.09
0.8-0.9	0.93 ± 0.09	0.27 ± 0.03	0.45 ± 0.21	0.13 ± 0.06	0.36 ± 0.22	0.10 ± 0.06
0.9-0.95	1.59 ± 0.24	0.52 ± 0.08				

Table 3

Values of b from a fit of the ϕ decay angular distribution in the helicity system to $a \cdot (1+b \cos^2 \theta_H)$. Comparison is made with the results of a previous experiment (WA4) [4]

Experiment	x_F range	b
WA57	$0.1 \leq x_F \leq 0.95$	-0.16 ± 0.07
	$0.7 \leq x_F \leq 0.95$	-0.86 ± 0.09
	$0.1 \leq x_F < 0.7$	-0.07 ± 0.08
WA4	$0.2 \leq x_F < 0.7$	-0.31 ± 0.09
	$0.7 \leq x_F \leq 1.0$	-0.89 ± 0.08

Table 4

Strange particles photoproduced in association with the ϕ

a) Numbers of events integrated over the whole photon energy range (20-70 GeV)

Reaction	No. of events
$\gamma p \to \phi + (\geq 1\ K^+) + X$	351 ± 26
$\gamma p \to \phi + (\geq 1\ K^-) + X$	203 ± 20
$\gamma p \to \phi + (\geq 1\ K^\circ_S) + X$	37 ± 10
$\gamma p \to \phi + (\geq 1\ \Lambda) + X$	7 ± 6

b) Numbers of $\phi K^\pm$ events as a function of the photon energy

Reaction	Photon energy range (GeV) 20-35	35-50	50-70
$\gamma p \to \phi + (\geq 1\ K^+) + X$	67 ± 12	182 ± 21	127 ± 16
$\gamma p \to \phi + (\geq 1\ K^-) + X$	14 ± 8	126 ± 14	99 ± 17

Figure captions

Fig. 1 : Mass distribution of K^+K^-; the curves show the result of the fit (explained in the text). Full curve: total fit, dashed curve: background, dashed-dotted curve: resonance signal.

Fig. 2 : Mass distributions of a) π^-K^+ and b) π^+K^-; the curves show the results of the fit (explained in the text). Full curve: total fit, dashed curve: background, dashed-dotted curve: resonance signal. The insets show enlarged the mass region of the $K^*(1420)$ (fitted background subtracted).

Fig. 3 : The number of a) ϕ, b) $K^{*o}(890)$ and c) $\bar{K}^{*o}(890)$ as a function of the charged particle multiplicity NCT. The curves show the geometrical trigger acceptance. For comparison the black boxes in a) indicate the shape of the distribution for inclusive photoproduction of ρ^o [1] (arbitrary normalization).

Fig. 4 : The number of a) ϕ, b) $K^{*o}(890)$ and c) $\bar{K}^{*o}(890)$ as a function of m_X^2, the mass squared recoiling against the vector mesons. The curves show the geometrical trigger acceptance. For comparison the black boxes in a) indicate the shape of the distribution for inclusive photoproduction of ρ^o [1] (arbitrary normalization).

Fig. 5 : Non-invariant cross-section $d\sigma/dx_F$ of the ϕ. The lines are described in the text.

Fig. 6 : Non-invariant cross-section $d\sigma/dx_F$ of a) the $K^{*o}(890)$ and b) the $\bar{K}^{*o}(890)$. The lines are described in the text.

Fig. 7 : Cross-section ratio $d\sigma/dx_F$ $[K^{*o}(890)]/(d\sigma/dx_F)$ $[\bar{K}^{*o}(890)]$. The line is described in the text.

Fig. 8 : $d\sigma/dp_T^2$ distribution of the ϕ. The straight line represents an exponential fit described in the text.

Fig. 9 : Helicity angle cos θ_H distributions from the ϕ decay for a) the total x_F range $0.1 \leq x_F \leq 0.95$; b) $0.7 \leq x_F \leq 0.95$ and c) $0.1 \leq x_F < 0.7$. The curves correspond to a fit of the form $a \cdot (1+b \cos^2 \theta_H)$ (see text).

Fig. 10 : Some selected graphs contributing to the cross-section formula in the text for a) $V_\gamma(x_1) \cdot V_p(x_2)$, b) $S_\gamma(x_1) \cdot V_p(x_2)$, c) $V_\gamma(x_1) \cdot S_p(x_2)$, d) $S_\gamma(x_1) \cdot S_p(x_2)$. Full quark lines denote valence quarks, dashed quark lines denote sea quarks.

Fig. 11 : The non-diffractive part of the ϕ cross-section as a function of x_F in comparison with a quark fusion model prediction (see text).

Fig. 12 : Different contributions to the ϕ cross-section (full line) predicted by the quark fusion model. The contributions are:
from $V_\gamma(x_1) \cdot V_p(x_2)$ (- - - - - - - - -),
from $S_\gamma(x_1) \cdot V_p(x_2)$ (-.-.-.-.-.-.-.-.-),
from $V_\gamma(x_1) \cdot S_p(x_2)$ (. . . . . .) and
from $S_\gamma(x_1) \cdot S_p(x_2)$ (..............).

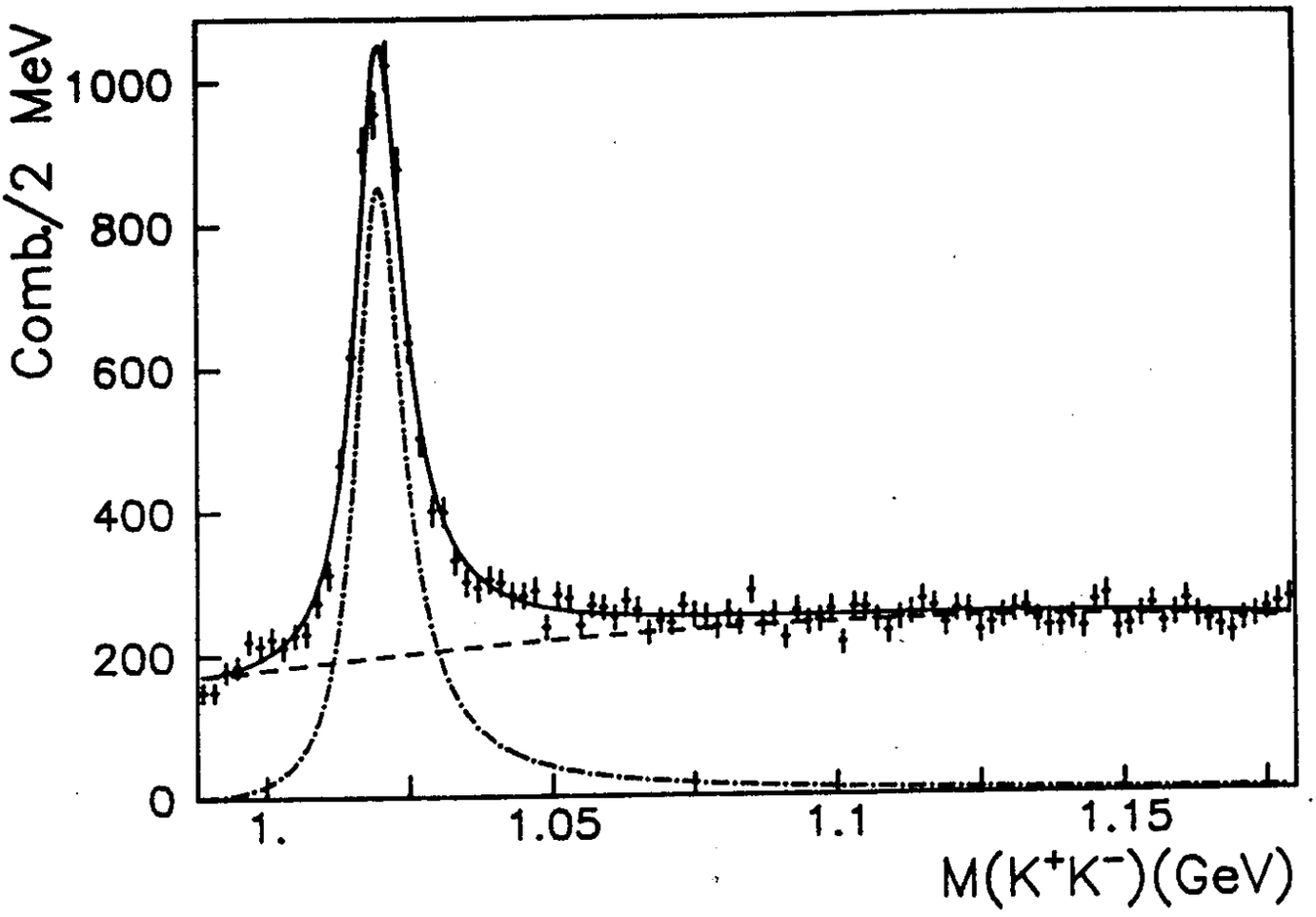

Fig. 1

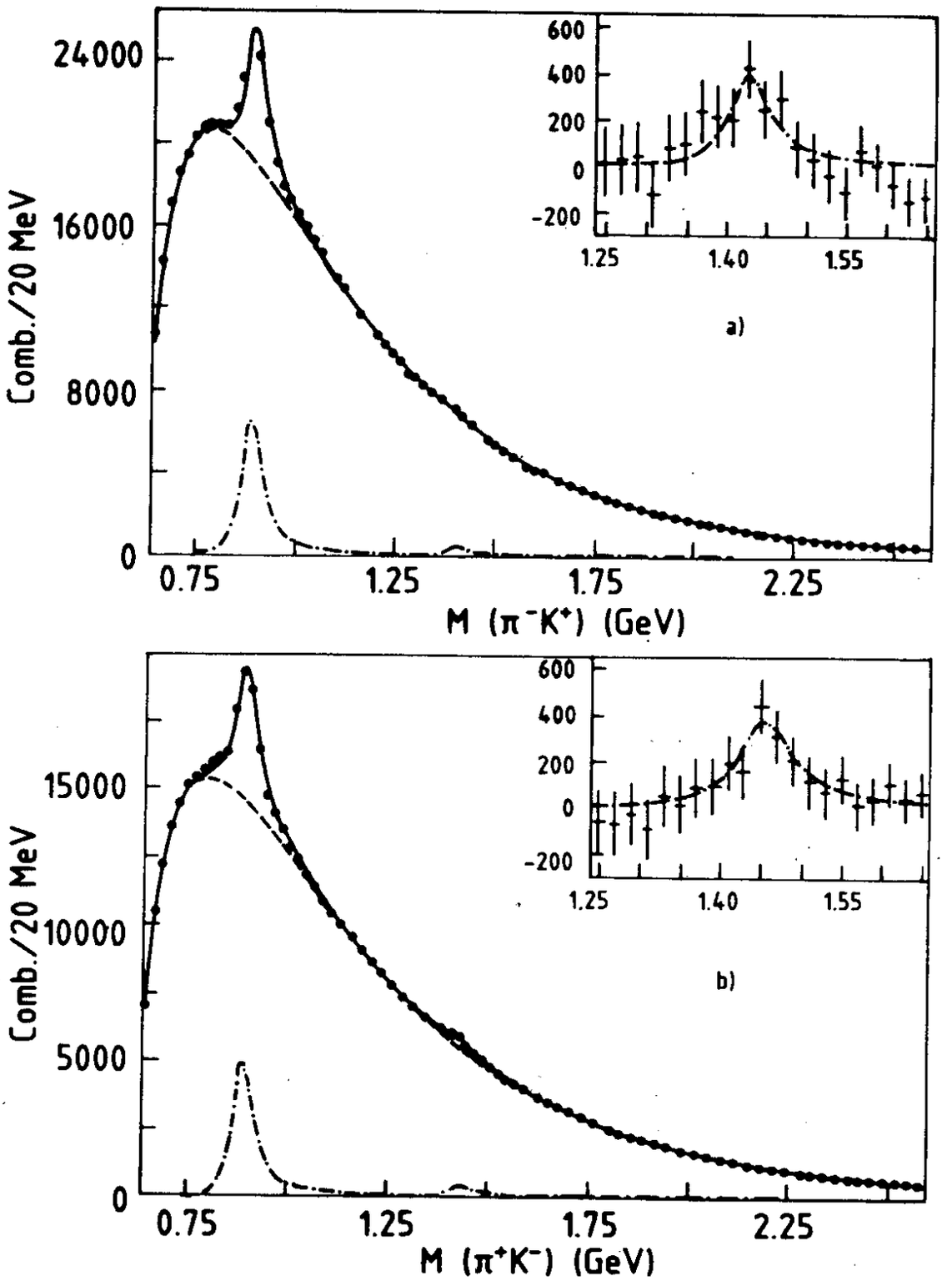
24000
16000
8000
0
Comb./20 MeV
0.75
1.25
1.75
2.25
M (π⁻K⁺) (GeV)
600
400
200
0
-200
1.25
1.40
1.55
a)
15000
10000
5000
0
Comb./20 MeV
0.75
1.25
1.75
2.25
M (π⁺K⁻) (GeV)
600
400
200
0
-200
1.25
1.40
1.55
b)

Fig. 2

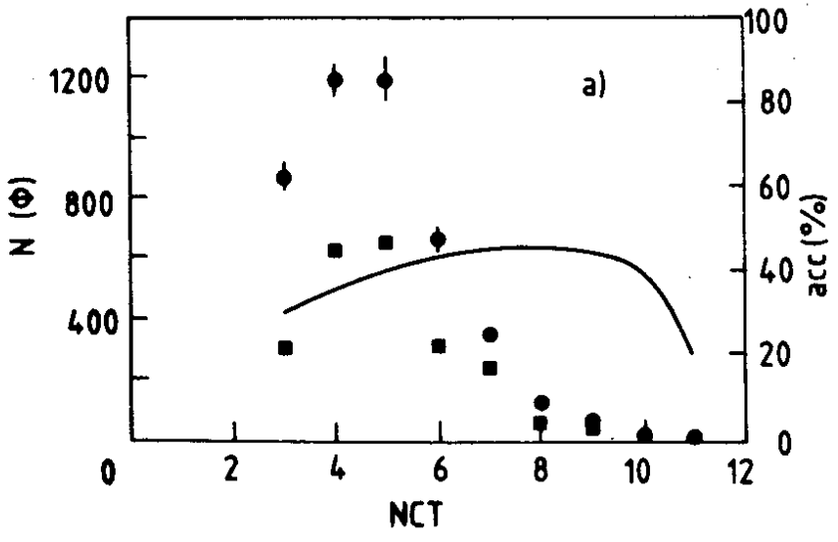
a)
N (Φ)
acc (%)
NCT
1200
800
400
100
80
60
40
20
0
0
2
4
6
8
10
12

Fig. 3

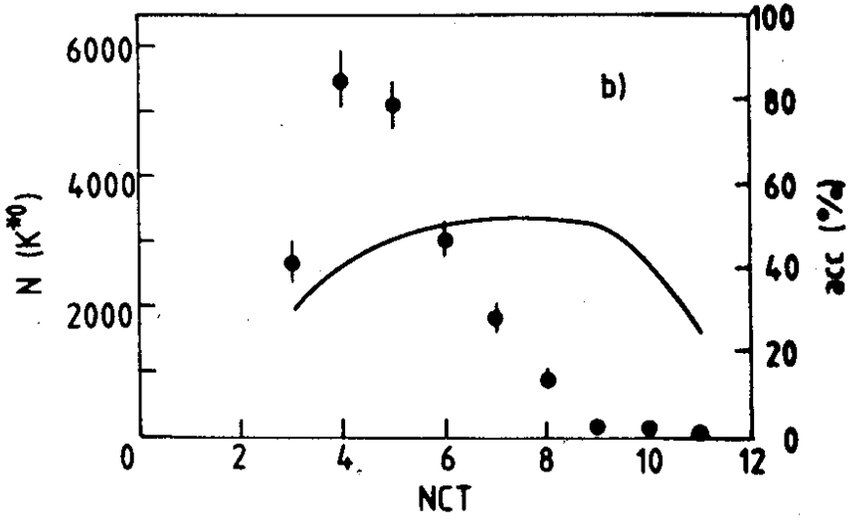
b)
N (K*0)
acc (%)
NCT
6000
4000
2000
100
80
60
40
20
0
0
2
4
6
8
10
12

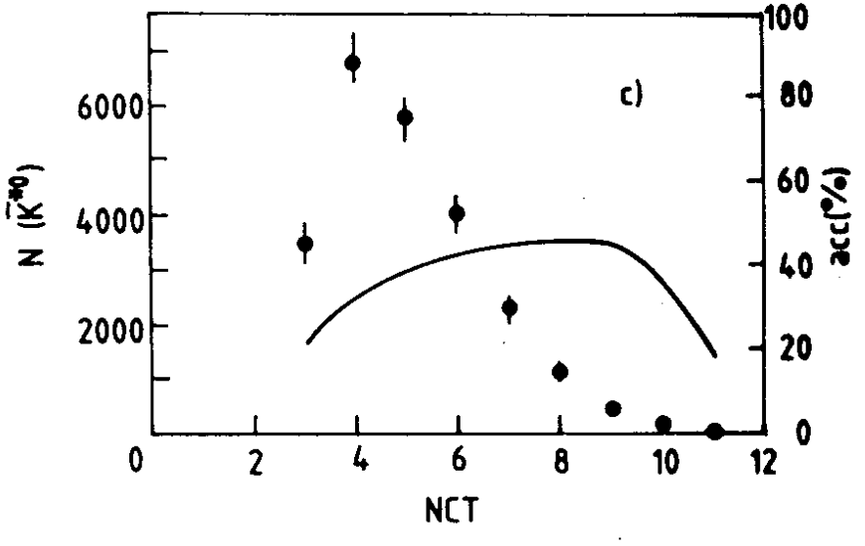
c)
N (K̄*0)
acc(%)
NCT
6000
4000
2000
100
80
60
40
20
0
0
2
4
6
8
10
12

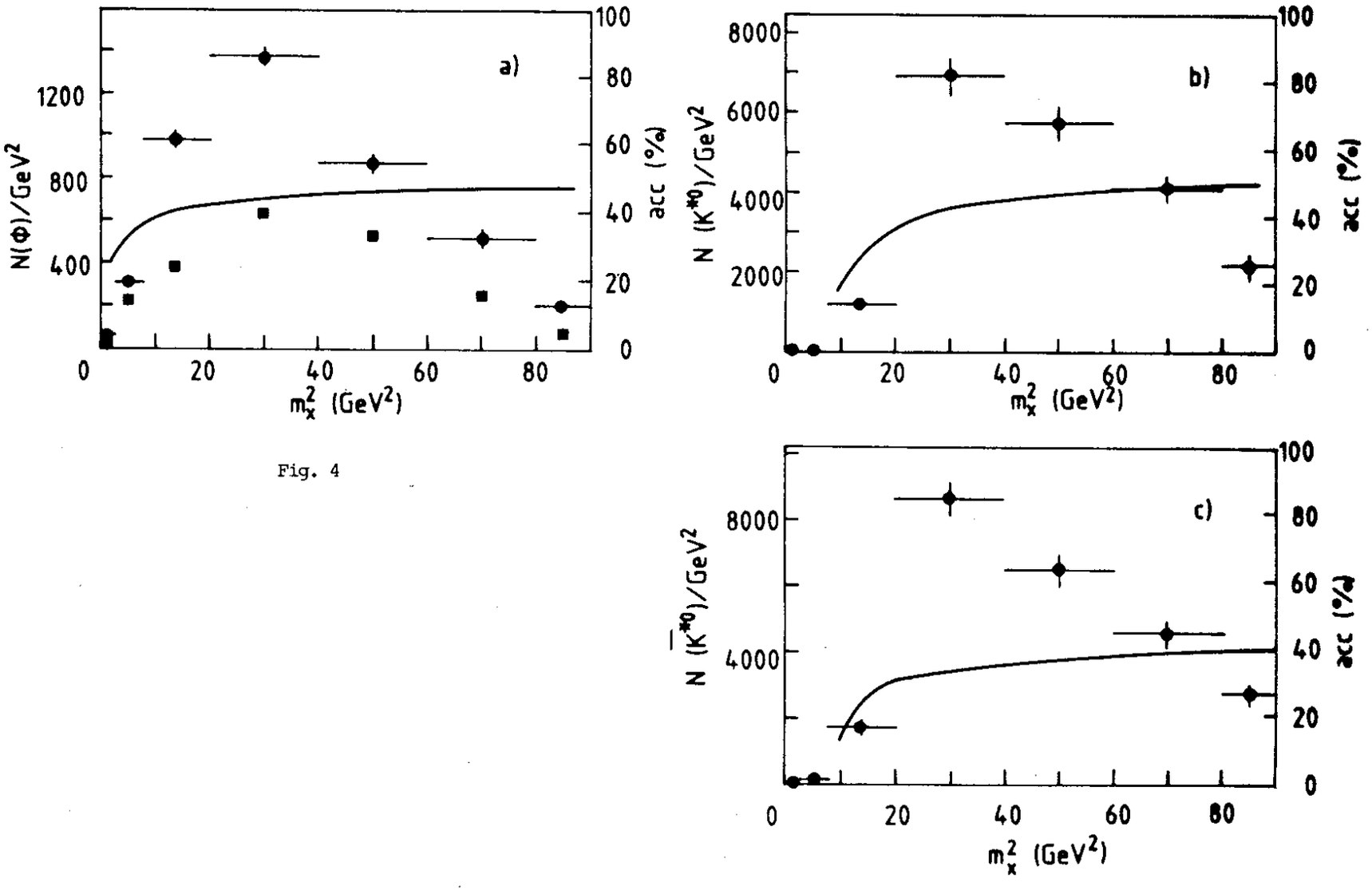
a)
b)
c)
N(Φ)/GeV²
N (K*0)/GeV²
N (K̄*0)/GeV²
acc (%)
m²x (GeV²)
0
20
40
60
80
400
800
1200
2000
4000
6000
8000
100

Fig. 4

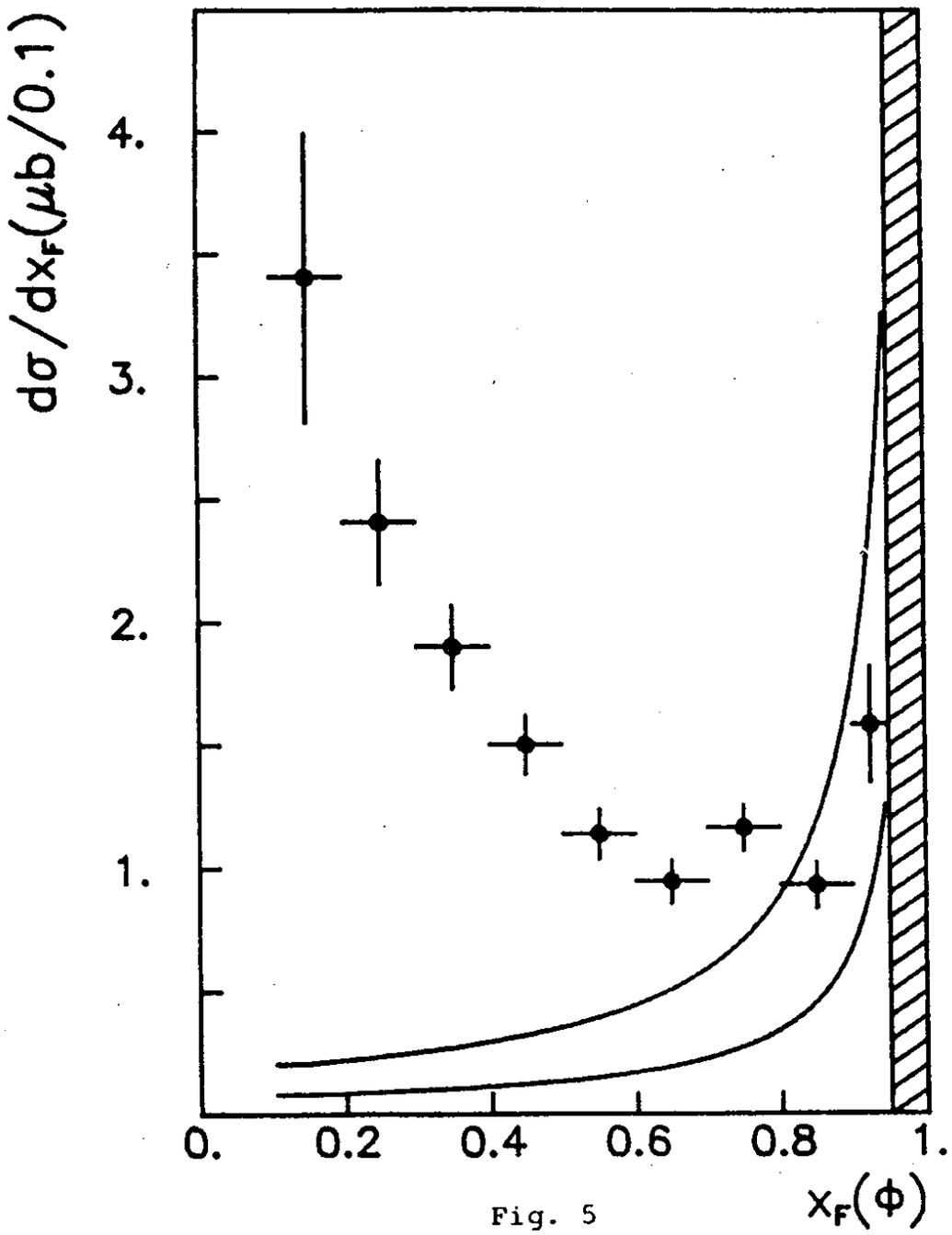

Fig. 5

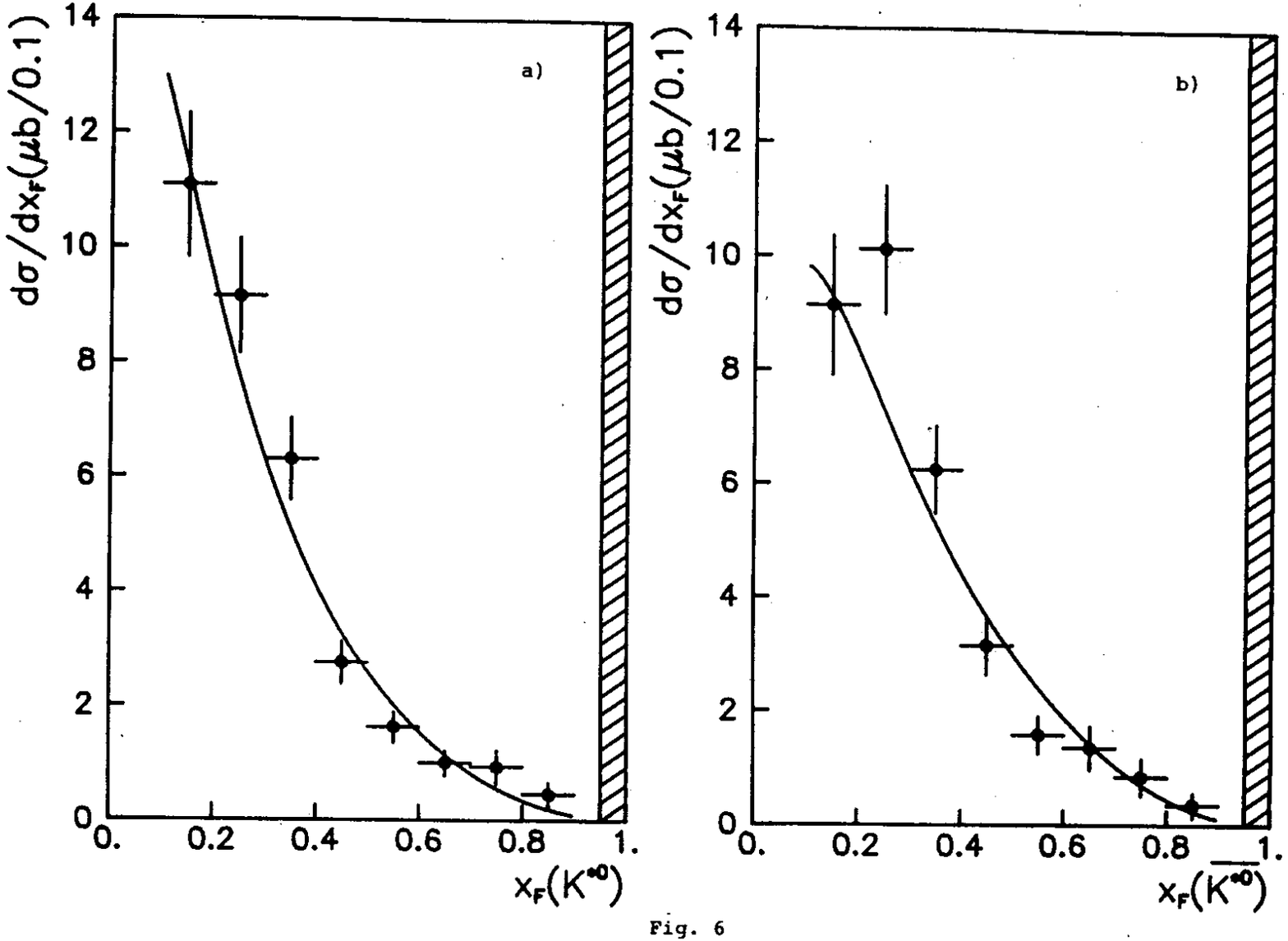

Fig. 6

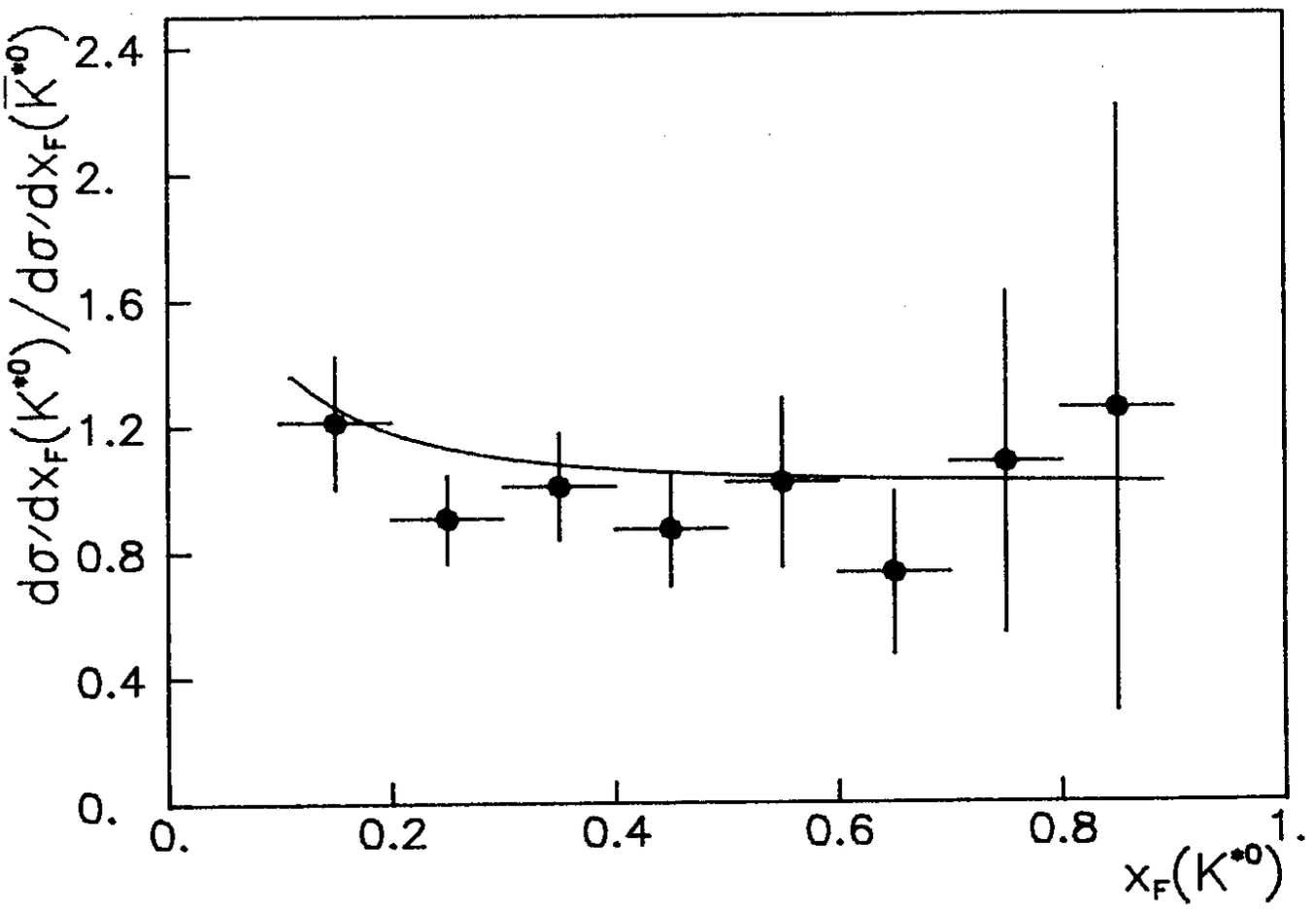
$d\sigma/dx_F(K^{*0})/d\sigma/dx_F(\bar{K}^{*0})$
2.4
2.
1.6
1.2
0.8
0.4
0.
0.
0.2
0.4
0.6
0.8
1.
$x_F(K^{*0})$

Fig. 7

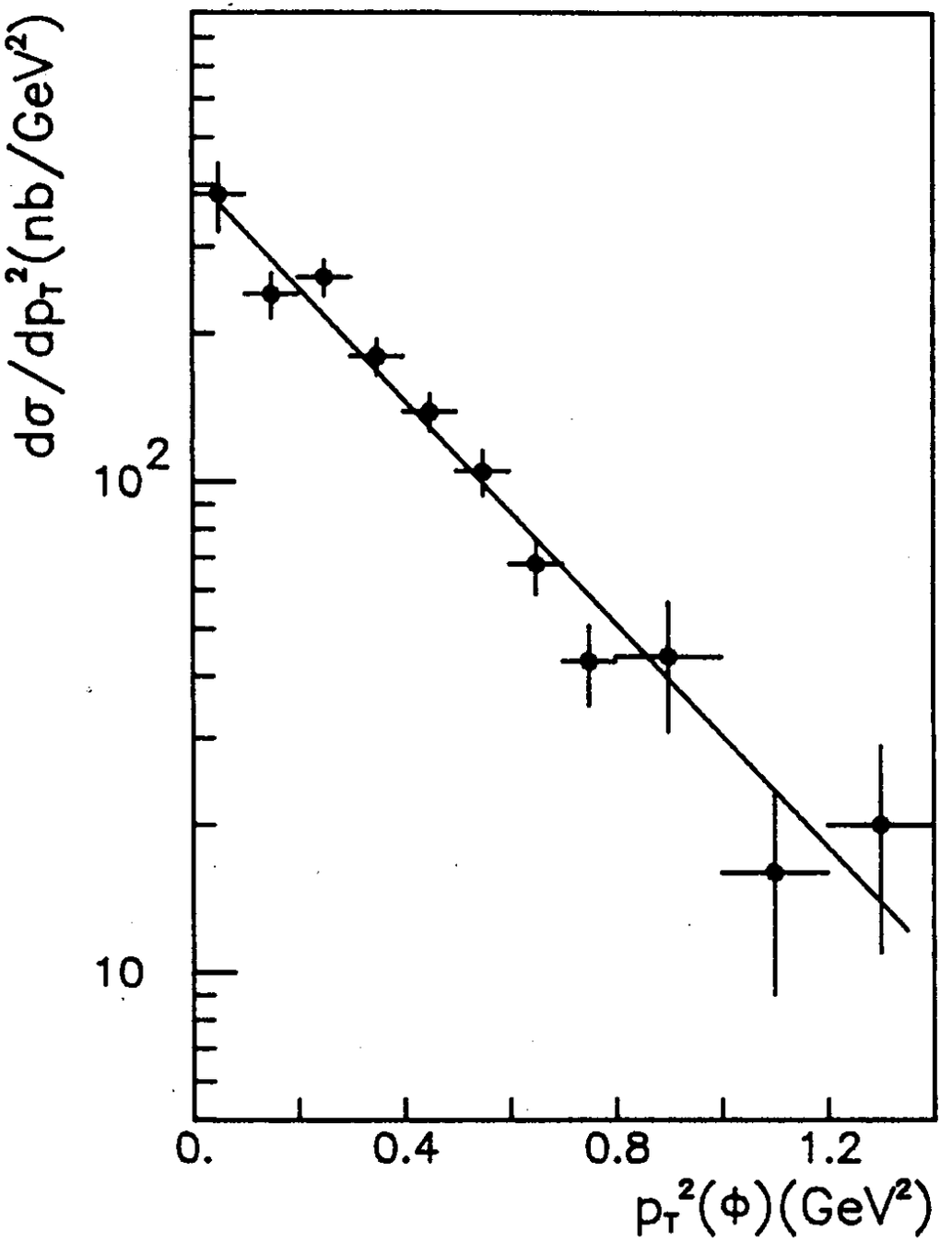

Fig. 8

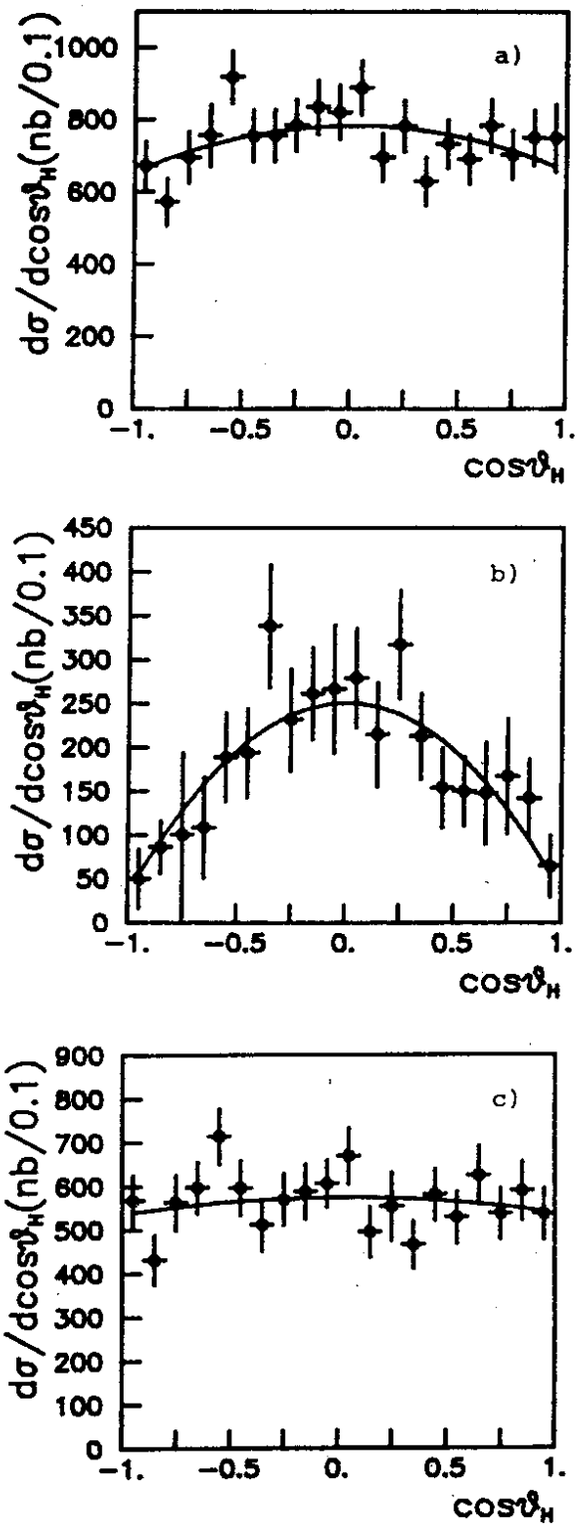
a)
b)
c)
$d\sigma/d\cos\vartheta_H$(nb/0.1)
$\cos\vartheta_H$
0
200
400
600
800
1000
50
100
150
200
250
300
350
400
450
-1.
-0.5
0.
0.5
1.

Fig. 9

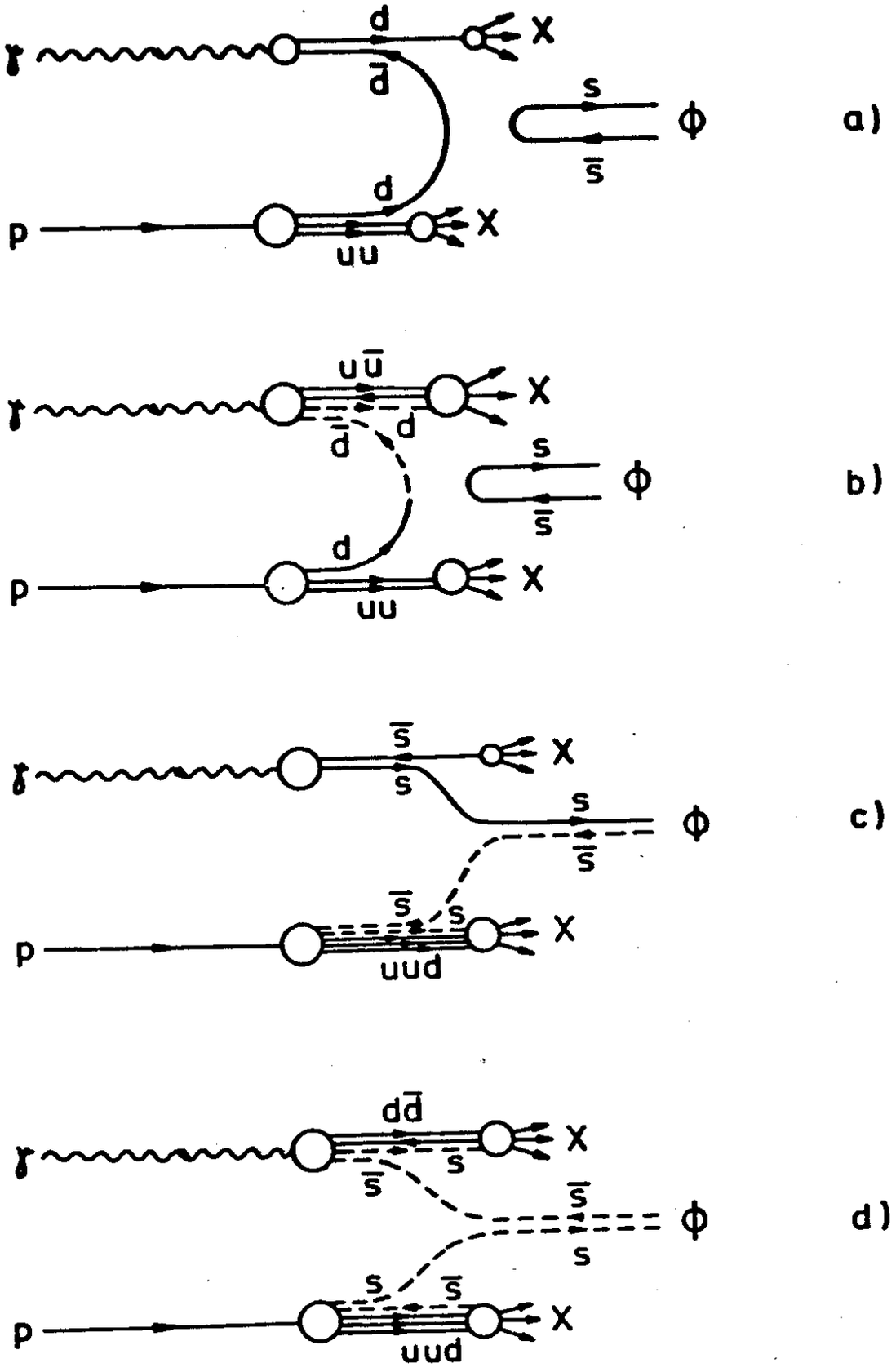
γ
d
X
d̄
s
φ
s̄
a)
d
p
X
uu
uū
X
d̄
d
s
φ
s̄
b)
d
p
X
uu
s̄
X
γ
s
s
φ
s̄
c)
s̄
s
p
X
uud
dd̄
X
γ
s̄
s
s̄
φ
s
d)
s
s̄
p
X
uud

Fig. 10

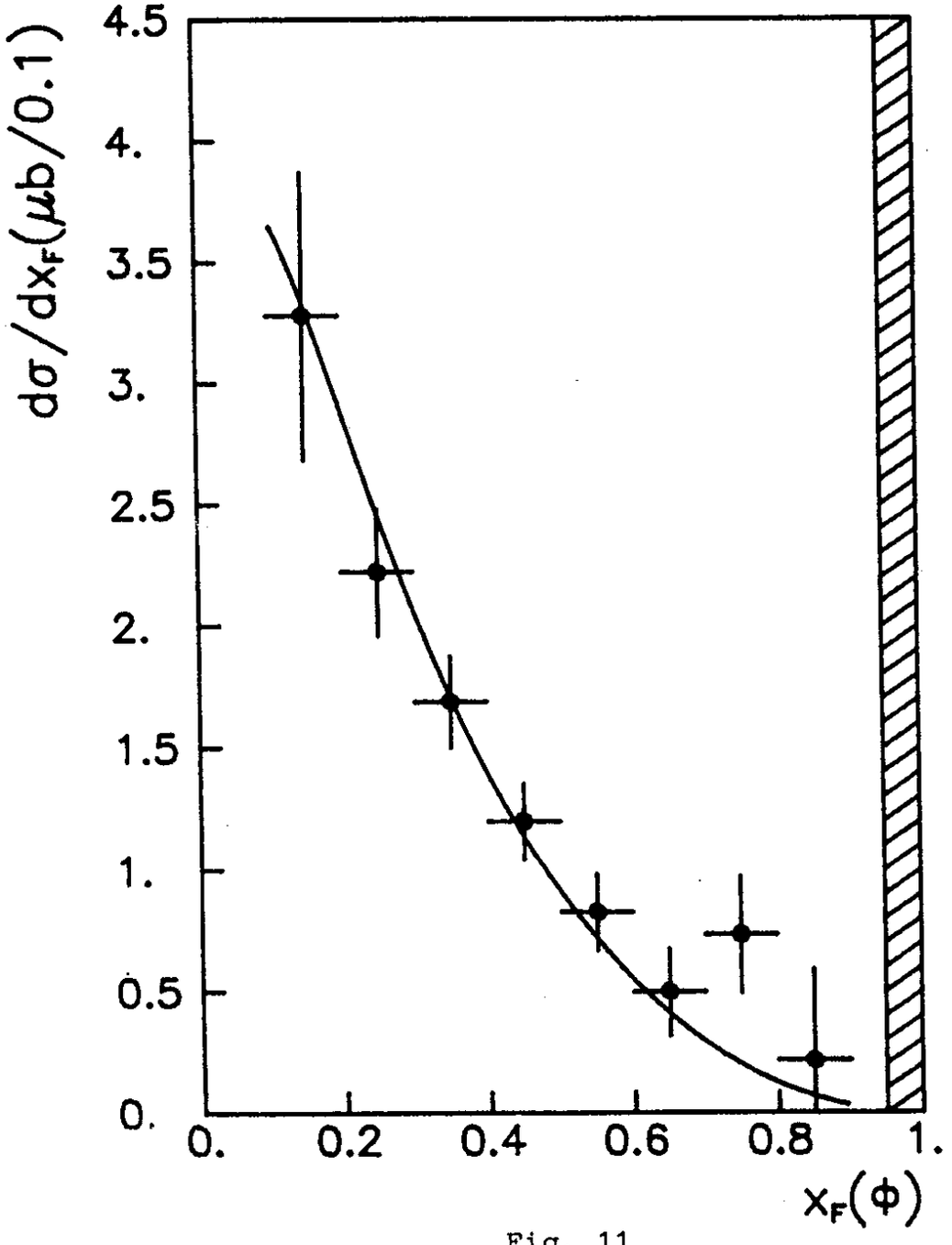

Fig. 11

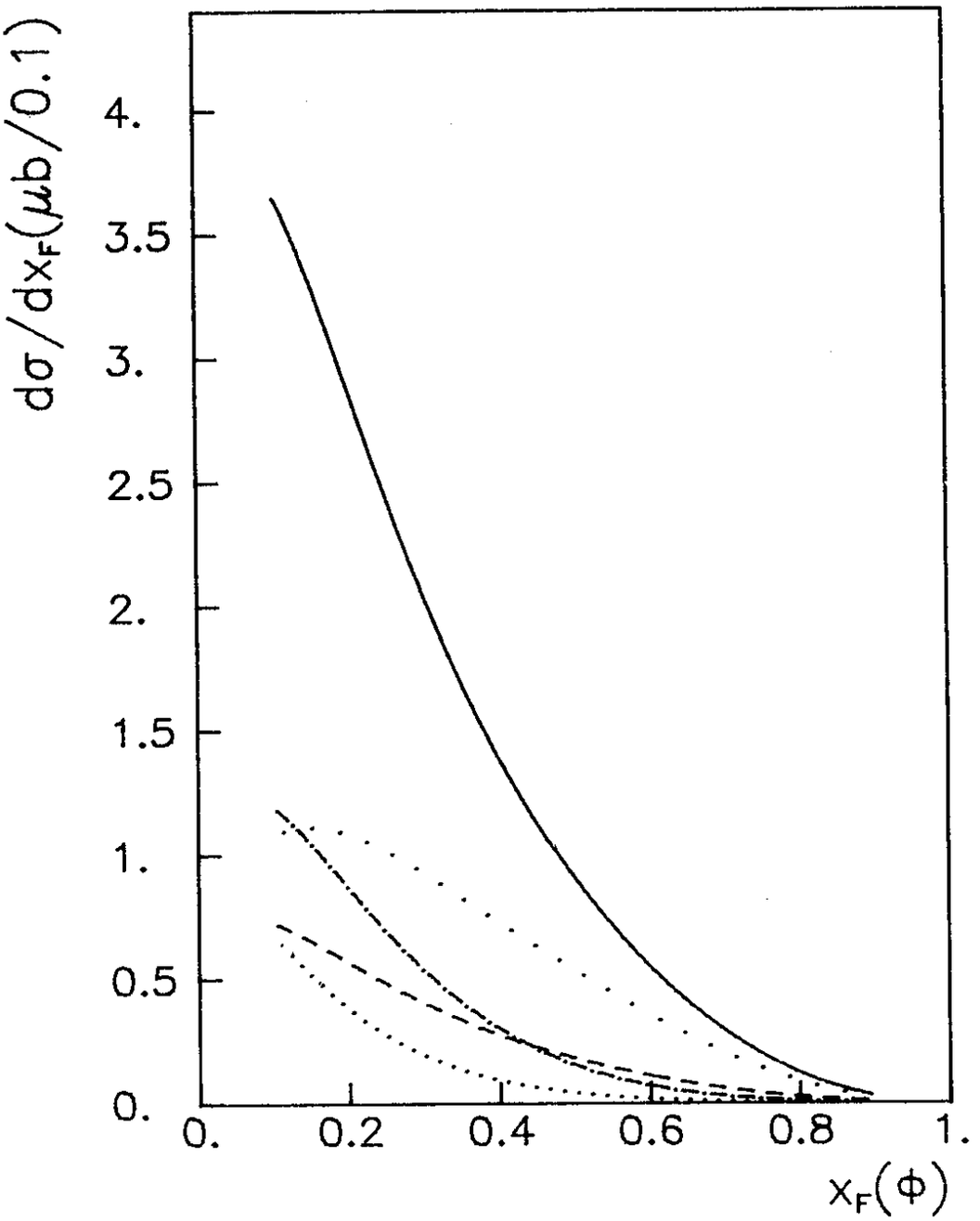

Fig. 12